JOURNAL OF THERMOPHYSICS AND HEAT TRANSFER
Vol. 20, No. 2, April–June 2006

Unsteady Laminar Buoyant Flow Through Rectangular Vents in Large Enclosures

Ranganathan Kumar,* Ahmad Sleiti,† and Jayanta Kapat‡
University of Central Florida, Orlando, Florida 32816

This computational study concentrates on transient laminar flow of air through rectangular vents in horizontal partitions between two large enclosures. For a vent aspect ratio of 1, three flow regimes were identified as the Rayleigh number (Ra) was varied from 1×10^3 to 5×10^4 based on flow parameters in the vent and corresponding modes of heat transfer through it. The Rayleigh number was found to be the critical control parameter, which determined the flow regimes of conduction, countercurrent, and oscillatory flow regimes. As the effective driving potential decreased with time, flow changed from one regime to the other so that higher-Rayleigh-number results showed all three regimes over time. Circulation patterns within the vent for the conduction regime ($Ra < 1500$) appeared to follow Chandrasekhar's well-known linear stability results. At higher Ra, sudden bursts of upflow with corresponding downflow have been documented and compared with experimental observations in the literature. The time traces of velocity and temperature fields for this flow regime reveal interesting mechanisms, which have been explained.

Nomenclature

D	=	width of the vent
g	=	acceleration due to gravity
$H1$	=	width of the enclosure
$H2$	=	height of the enclosure
L	=	height of the vent
L/D	=	vent aspect ratio
Nu	=	Nusselt number
P	=	dimensionless pressure $= p/(\rho\alpha^2/L^2)$
Pr	=	Prandtl number
p	=	total pressure less hydrostatic pressure
Ra	=	Rayleigh number $= g\beta\Delta T L^3/\nu\alpha$
Ra_{critical}	=	critical value of Ra for onset of flow through the vent
Re_Δ	=	densimetric Reynolds number $= V_\Delta H/\nu$
T	=	temperature
T_{cold}, T_c	=	initial temperature of fluid in upper chamber
T_{hot}	=	initial temperature of fluid in lower chamber
T_{ref}	=	reference temperature
t	=	time
t_c	=	time constant
U, V	=	dimensionless components of velocity in x and y directions, respectively
u, v	=	components of velocity in x and y directions, respectively
X, Y	=	dimensionless horizontal and vertical coordinates
x, y	=	horizontal and vertical coordinates
α	=	thermal diffusivity of the fluid
β	=	coefficient of thermal expansion of the fluid
ΔT_i	=	initial temperature difference between upper and lower chamber
θ	=	dimensionless temperature $= (T - T_{\text{ref}})/\Delta T_i$
$\theta_{\text{av}} = [T(t)_{\text{av}} - T_c]/\Delta T_i$	=	instantaneous averaged nondimensionalized temperature on left and right sidewalls
$\theta_b = [T(t)_b - T_c]/\Delta T_i$	=	instantaneous bulk (mass-weighted average) nondimensionalized temperature along a cross section on the center of the vent at $L/2$
ν	=	kinematic viscosity of the fluid
ρ_o	=	reference density of the fluid
$\tau = t\alpha/L^2$	=	dimensionless time
$\Psi_b = V_{\text{bmag}}/V_{\max}$	=	instantaneous mass-weighted average velocity magnitude along a cross section located at the center of the gap, i.e., at $L/2$
$\Psi_c = V_y/V_{\max}$	=	instantaneous vertical velocity at a point located at the center of the vent, i.e., at $D/2$ and $L/2$

Introduction

THE problem of natural convection heat and mass transfer has been studied extensively by many authors.[1] The problem of natural convection in enclosures with the top plate colder than the bottom plate has been treated extensively in the literature as well. However, the problem of a heavier fluid on top of a lighter fluid separated by a narrow vent has not been dealt with analytically or numerically. Such a flow configuration occurs in buildings where elevator shafts, stairwells, service shafts, and the like can act as vents connecting two floors. The flow in these vents is buoyancy-generated due to a fire in the bottom enclosure or to leakage of contaminant gases. This transient flow may have several modes and the heat-transfer mechanism is of interest, especially when the flow becomes oscillatory.

Flow through apertures connecting two enclosures has been a subject of study for more than four decades. Early studies were limited to openings in vertical partitions. The fundamental difference between

Received 10 November 2004; revision received 4 March 2005; accepted for publication 7 March 2005.

*Professor, Department of Mechanical, Materials and Aerospace Engineering, 4000 Central Florida Boulevard.

†Research Scholar/Scientist and Instructor, Department of Mechanical, Materials and Aerospace Engineering, 4000 Central Florida Boulevard. Member AIAA.

‡Associate Professor, Department of Mechanical, Materials and Aerospace Engineering, 4000 Central Florida Boulevard. Associate Fellow AIAA.

flow through a vent in a vertical partition and flow through a vent in a horizontal partition is the stable stratification of fluid in the former case, whereas the configuration is unstable for the latter. In spite of this fundamental difference, these studies offer a unique insight into flow mechanisms through apertures and different methodologies available to model them. Some prominent studies are reported here.

Prahl and Emmons[2] conducted an experimental and theoretical study of fire-induced flow through an opening in a vertical partition. The experiments involved steady flows through a single opening with a reduced-scale kerosene/water analog. Inflow and outflow orifice coefficients were determined and found to be significantly different at low values of Reynolds number based on flow height but reached an asymptotic value of approximately 0.68 at high values of Reynolds number.

In the same year Leach and Thompson[3] carried out an experimental investigation of flows in horizontal circular tubes. For the whole range of $0.5 \le L/D \le 9.4$ and $3 \times 10^4 \le Re \le 1.5 \times 10^5$ investigated, they found that $C_D = 0.09$, a constant independent of L/D and Re_Δ. A large-scale experiment with carbon dioxide and water as working fluids was used to verify these results for gases. They also investigated the forced-flow rate requirements to prevent countercurrent flow in the tube.

Brown[4] was the first to study flow through square openings in horizontal partitions with heavier fluid above the partition, both analytically and experimentally. In his analysis, he assumed that all heat transfer was due to advection only and no mixing occurred within the vent. Assuming friction to be negligible, he invoked the Bernoulli equation to predict that the Nusselt number is proportional to the product of the square root of the Grashof number and the Prandtl number, the reference length being the height of the vent. Brown and Salvason[5] did a similar analysis for a vent in a vertical partition to derive a theoretical relationship between Nu and Gr.

An experimental study of buoyancy-driven exchange flow through small openings in horizontal partitions for the same geometric configuration as this study was reported by Epstein.[6] The experimental apparatus consisted of two enclosures, one on top of the other, with brine and fresh water as working fluids. The study concentrated on finding the effect of height-to-diameter aspect ratio of the vent (L/D) on the dimensionless exchange flow rate as defined by Mercer and Thompson[7] in their study on inclined ducts. Four different flow regimes were identified as L/D was varied from 0.01 to 10. The first of these was named the oscillatory exchange-flow regime where plumes of fluids periodically broke through the opening. He used Taylor's wave theory to predict the motion of the interface and showed that the Froude number is a constant for this regime. The second flow regime was called the Bernoulli flow regime due to the fact that data showed the same trends as predicted by Brown.[4] For this regime, he found that Froude number $Q = 0.23(L/D)^{1/2}$ (length/width of the vent). For large L/D, the flow rate was observed to be smaller than the other two regimes due to violent mixing within the vent. He used an analysis similar to that reported by Gardner[8] to provide correlations for his regime. An intermediate regime was also identified having combined characteristics of turbulent diffusion and Bernoulli flow.

A brine–water analog was also studied experimentally by Conover and Kumar.[9] Conover et al.[10] studied experimentally the buoyant countercurrent exchange flow through a vented horizontal partition using a two-component laser Doppler velocimeter. Detailed measurements of velocity were made a small distance above a circular tube with an aspect ratio of 1. Even for this aspect ratio and a Reynolds number ranging between 2.4×10^3 and 7.7×10^3, the mixing in the vent was found to be turbulent and unsteady. He also found that the flow coefficient was nearly constant for a Reynolds number as low as 2.4×10^3. This finding was in contrast with the work of Stecker et al.,[11,12] who showed that exchange flows reached self-similarity only for Reynolds numbers greater than 10^4. Tan and Jaluria[13] and Jaluria et al.[14] studied cases where the vent flow was governed by both pressure and density differences across the vent.

Myrum[15] conducted heat-transfer experiments using water in a top-vented enclosure heated by a disk on the enclosure floor. He observed four modes of flow, which were unstable and oscillated randomly from one to the next. More on this flow situation will be given in the results and discussion section.

A numerical study of unsteady buoyant flow through a horizontal vent placed slightly asymmetrically between two enclosed vents was performed by Singhal and Kumar.[16]

In all the studies discussed, only high-Ra-number ranges were investigated so that the effect of viscosity could be neglected, and, in general, flow coefficient or Froude number was considered a function of L/D only, independent of the driving potential. Also, the scaled brine–fresh water models used may not give results comparable to those of full-scale air models due to large changes in the Prandtl number and Schmidt number at low Ra. Therefore, these models may not be applicable to the range of Ra investigated in this study.

The objective of this study is to identify the different flow regimes encountered for low to high Rayleigh number in a vented enclosure and to discuss the physical mechanisms using the time trace of temperature and fluid flow results for a vent aspect ratio of 1.

Governing Equations and Formulation

Time-dependent governing equations for the laminar, two-dimensional flow were derived from fundamental laws of conservation of mass, momentum, and energy as follows:

$$\frac{\partial \rho}{\partial t} + \frac{\partial(\rho u)}{\partial x} + \frac{\partial(\rho v)}{\partial y} = 0 \tag{1}$$

$$\rho\left(\frac{\partial u}{\partial t} + u\frac{\partial u}{\partial x} + v\frac{\partial u}{\partial y}\right) = -\frac{\partial p}{\partial x} + \mu\left(\frac{\partial}{\partial x}\left(2\frac{\partial u}{\partial x} - \frac{2}{3}(\nabla \cdot \vec{v})\right) + \frac{\partial}{\partial y}\left(\frac{\partial u}{\partial y} + \frac{\partial v}{\partial x}\right)\right) \tag{2}$$

$$\rho\left(\frac{\partial v}{\partial t} + u\frac{\partial v}{\partial x} + v\frac{\partial v}{\partial y}\right) = -\frac{\partial p}{\partial y} + \mu\left(\frac{\partial}{\partial y}\left(2\frac{\partial v}{\partial y} - \frac{2}{3}(\nabla \cdot \vec{v})\right) + \frac{\partial}{\partial y}\left(\frac{\partial u}{\partial y} + \frac{\partial v}{\partial x}\right)\right) + \rho g \tag{3}$$

$$\frac{\partial T}{\partial t} + u\frac{\partial T}{\partial x} + v\frac{\partial T}{\partial y} = \alpha\left(\frac{\partial^2 T}{\partial x^2} + \frac{\partial^2 T}{\partial y^2}\right) + \frac{\beta T}{\rho C_p}\left(\frac{\partial p}{\partial t} + u\frac{\partial p}{\partial x} + v\frac{\partial p}{\partial y}\right) \tag{4}$$

The variables L and α/L are used to normalize length and velocity respectively, α/L^2 to nondimensionalize time, and ΔT_i to nondimensionalize temperature.

The transient calculation approach considered in this study is not using the Boussinesq model, which treats density as a constant value in all solved equations, except for the buoyancy term in the momentum equation. Instead, the approach used here is that the initial density is computed from the initial pressure and temperature, so the initial mass is known. As the solution progresses over time, this mass will be properly conserved. When this approach is used the operating density, ρ_o, appears in the body-force term in the momentum equation as $(\rho - \rho_o)g$. The definition of the operating density ρ_o is thus important for this buoyancy driven flow.

No-slip conditions were used for velocity boundary conditions at all walls, including the vent walls. Initially fluid is at rest everywhere in the domain; therefore velocity components were set equal to zero at nondimensionalized time $\tau = 0$. All the walls were treated adiabatically and hence the normal gradients of temperature were set equal to zero at all fluid–wall interfaces. At $\tau = 0$, the lower chamber contains hot fluid with $\theta = 1$, whereas the upper chamber and the vent contain cold fluid with $\theta = 0$. The flow parameters of interest are Ra and Pr. Pr is maintained constant at 0.7. Referring to Fig. 1, the geometric parameters are vent aspect ratio, L/D, $H1/L$, and the

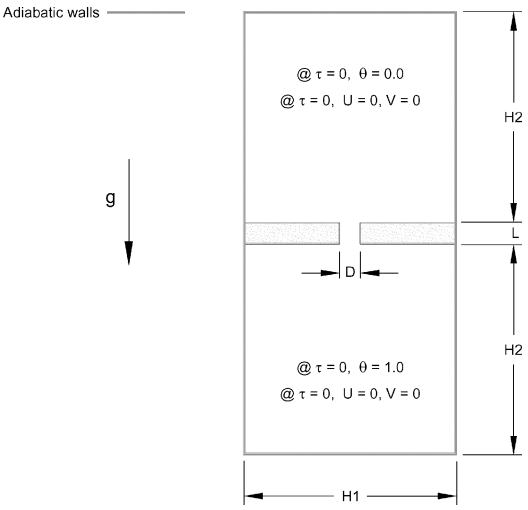

Fig. 1 Schematic diagram of the model.

enclosure aspect ratio, $H1/H2$. In this study these parameters are fixed at 1, 10, and 1 respectively. Although the problem of natural convection in a horizontal cavity with bottom heating is highly three-dimensional, it can be treated as a two-dimensional problem for very long vents, which is the case considered in this paper.

Numerical Procedure

Equations (1) through (4) are discretized over the computational domain using a control volume approach as documented by Patankar.[17] The resulting algebraic equations for velocity components and temperature were solved using the SIMPLE algorithm, which involves the use of pressure correction equations to enforce mass conservation. The FLUENT code is used for this simulation. A segregated solver with first-order implicit unsteady formulation is employed for this study. The air properties, density, thermal conductivity, specific heat, and dynamic viscosity, are varied as piecewise functions of temperature. By default, the solver will compute the operating density, ρ_o, which appears in the body-force term in the momentum equations as $(\rho - \rho_o)g$, by averaging over all cells. The discretization schemes used are second-order for pressure, SIMPLE for pressure–velocity coupling, and second-order upwind for momentum and energy. The underrelaxation factor is 0.3 for pressure, 1 for density, body forces, and energy, and 0.7 for momentum. The code was tested against certain benchmark solutions to validate the results. For the unsteady case, results obtained by Patterson and Imberger,[18] and for the steady case, results obtained by Davis[19] were selected for comparison with the results predicted. Both these papers deal with enclosure geometries with heated and cooled vertical walls and adiabatic bottom and top walls. The predicted results were within 3% of these benchmark solutions.

Figure 2 shows the numerical grid generated for this study using the Gambit grid generator. Because FLUENT is an unstructured solver, it uses internal data structures to assign an order to the cells, faces, and grid points in a mesh and to maintain contact between adjacent cells. It does not, therefore, require i, j, k indexing to locate neighboring cells. This gives the flexibility to use the grid topology that is best for the problem, because the solver does not force an overall structure or topology on the grid. For the two-dimensional problem considered here, quadrilateral cells are used to form a multiblock structured mesh. More details on grid generation are provided in the FLUENT documentation. A grid-independent study is performed using three nonuniform grid distributions: coarse grid with 91×63 grid points used for every enclosure and 21×13 grid points used for the vent, medium grid with 133×91 grid points used for every enclosure and 31×19 grid points used for the vent, and fine grid with 201×135 grid points used for every enclosure and 47×29 grid points used for the vent. The results for temperature and the two components of velocity at the center of the vent and at different locations inside the two enclosures for different Ra values were

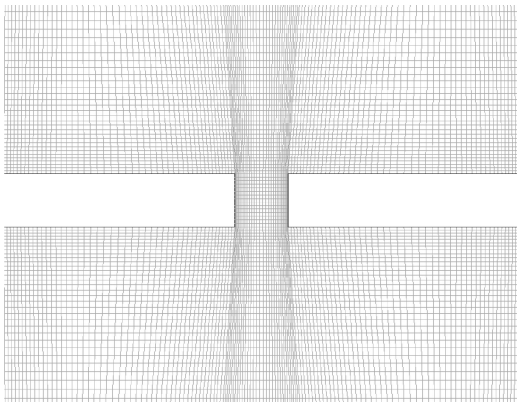

Fig. 2 Numerical grid.

compared using all three grids. The maximum difference in temperature and velocities between coarse and medium grids found to be less than 1.5% when results from both grids are compared over the full time domain. The maximum difference between medium and fine grids was found to be less than 0.2%. Finally, the nonuniform grid of 133×91 grid points was used for every enclosure and a grid of 31×19 grid points was selected for the vent with seven grid points placed near every sidewall inside the boundary layer. One complete unsteady solution for one geometry and average Rayleigh number involved computation of up to 70,000 time steps with approximately 30 to 40 iterations for every time step to have more confidence in results, although a convergence usually was achieved after 10 to 15 iterations.

Convergence criteria were set to ensure converged results for continuity, X-velocity, Y-velocity, and energy. A solution was assumed converged if the maximum scaled residuals of the continuity, X-velocity, Y-velocity, and energy were equal to 10^{-4}, 10^{-5}, 10^{-6}, and 10^{-7}, respectively. The residual is scaled using a scaling factor representative of the flow rate of ϕ through the domain. This "scaled" residual is defined as

$$R^{\phi} = \frac{\sum_{\text{cells}\,P} \left| \sum_{nb} a_{nb}\phi_{nb} + b - a_P\phi_P \right|}{\sum_{\text{cells}\,P} |a_P\phi_P|} \tag{5}$$

For the momentum equations the denominator term $a_P\phi_P$ is replaced by $a_P v_P$, where v_P is the magnitude of the velocity at cell P.

The scaled residual is a more appropriate indicator of convergence. For the continuity equation, the solver's scaled residual is defined as

$$R^{c}_{\text{iteration}\,N} \Big/ R^{c}_{\text{iteration}\,5} \tag{6}$$

The denominator is the largest absolute value of the continuity residual in the first five iterations.

For the enclosure under consideration, a fixed time-stepping method is used for a time-marching scheme. The time step used was based on estimating the time constant as[20]

$$t_c = L/U \approx (L^2/\alpha)(PrRa)^{-\frac{1}{2}} = L\Big/\sqrt{g\beta\Delta T_i L}$$

where L and U are the length and the velocity scales, respectively.

Then a time step is determined such that $\Delta t = t_c/20$. Note that this time-step value used in this study is five times less than the time step recommended in the open literature to ensure time convergence. After oscillations with a typical frequency have decayed, the solution reaches steady state.

The time-step independence was tested prior to obtaining a solution for the desired problem. The time-independent study is established by tracking the changes in temperature and the two components of velocity at a point located at the center of the vent by increasing and decreasing the time step for all cases of Ra studied. Decreasing the time step from $\Delta t = t_c/20$ to $\Delta t = t_c/25$ resulted in less than 0.05% difference in temperature and velocities when

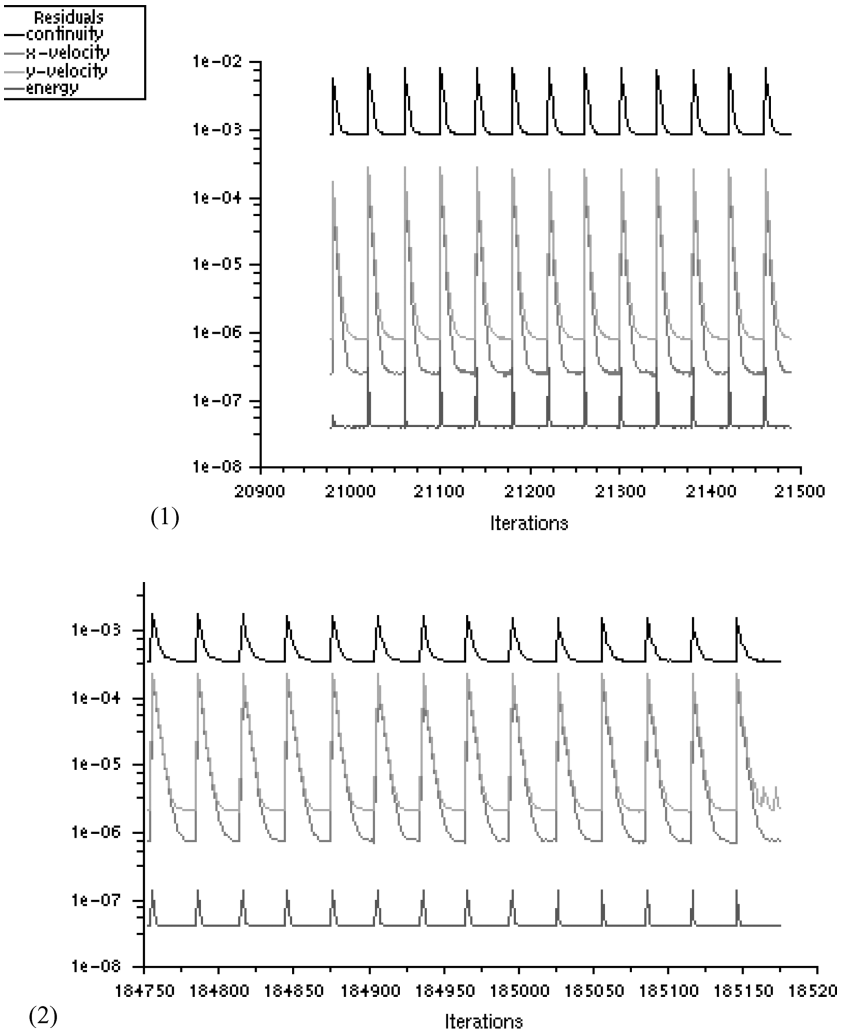

Fig. 3 Scaled residuals for *Ra* = 2500, time = 250 s 1) and for *Ra* = 10000, time = 4616 s 2).

results from both time steps are compared over the full time domain. Increasing the time step from $\Delta t = t_c/20$ to $\Delta t = t_c/15$ resulted in less than 0.1% difference in temperature and velocities when results from both time steps are compared over the full time domain. Based on this, the time step used for all simulations is $\Delta t = t_c/20$. Figure 3 shows sample convergence plots of the scaled residual for Ra of 2,500 and 10,000, respectively, at different time steps.

Quantities of Interest

The Rayleigh number was defined as $Ra = (g\beta\Delta T_i L^3)/\nu\alpha$, where ΔT_i is the initial temperature difference between the two enclosures (i.e., at $\tau = 0$). As the interaction between the fluids in the two enclosures proceeds with time, the effective driving potential is the temperature difference across the vent and not ΔT_i. Magnitude of the temperature difference across the vent decreases with time. Therefore, new quantities need to be defined that would reflect this change in driving potential with time. To this end, we define the following quantities:

1) Instantaneous averaged nondimensionalized temperature (θ_{av}) on left and right side walls of the vent, defined as

$$\theta_{\text{av}} = \frac{T(t)_{\text{av}} - T_c}{\Delta T_i}$$

Thus (θ_{av}) will vary from 0 to 1.

2) Instantaneous bulk (mass-weighted average) nondimensionalized temperature (θ_b) along a cross section on the center of the vent at $L/2$ defined as

$$\theta_b = \frac{T(t)_b - T_c}{\Delta T_i}$$

Thus (θ_b) will vary from 0.0 to 1.0.

3) Instantaneous vertical velocity (Ψ_c) at a point located at the center of the gap, that is, at $D/2$ and $L/2$. This velocity is normalized by the maximum vertical velocity at the same location ($\Psi_c = V_y/V_{\max}$), where the maximum velocity is the highest velocity found in the domain at any time. Thus (Ψ_c) will vary from –1.0 to 1.0.

4) Instantaneous mass-weighted average velocity magnitude (Ψ_b) along a cross section located at the center of the gap, that is, at $L/2$. This velocity is normalized by the maximum velocity magnitude along the same location ($\Psi_b = V_{b\text{mag}}/V_{\max}$), where the maximum velocity magnitude is the highest velocity magnitude found on the domain at any time. Thus (Ψ_b) will vary from 0.0 to 1.0.

All quantities described above are then calculated at every time step throughout the simulation.

Results and Discussion

The interaction between the two enclosures takes place through the vent and the flow patterns within the vent determine the mode of heat transfer and the rates of heat and mass transfer across it. These flow patterns in the vent are dependent on the vent geometry, the magnitude of the buoyancy force which drives the flow across it, and to a great extent the flow patterns in the enclosures themselves.

The last category makes the flow configuration difficult to analyze. However, from the results presented, an attempt has been made to explain the localized phenomena. Based on the mode of heat transfer and the associated flow characteristics, three categories have been identified. These are the conduction regime, the countercurrent regime, and the oscillatory regime. The Rayleigh number, as will be explained, largely governs these regimes.

The Conduction Regime ($Ra \leq 1500$)

For small Rayleigh numbers, the buoyancy forces are not strong enough to overcome the viscous forces in the vent where the vertical walls of the vent are closer to each other as compared to the enclosure's vertical walls. Consequently, there is no bulk fluid motion within the vent, as shown by Fig. 4, and all the heat transfer is solely by conduction for $Ra \leq 1500$.

Flow patterns for this Ra at different time steps are given in Fig. 5. In this regime, the vent acts like a heater plate for the upper chamber, which is filled with colder fluid and as a cold plate for lower chamber, which is filled with warmer fluid. Thus, in the enclosures, bulk fluid motion ensues immediately after the initial establishment of a temperature gradient in vent. A plume rises steadily into the upper chamber, forcing the colder fluid to move along the sidewalls to replace the rising fluid, forming two cells of equal strength on either side of it. For a considerable length of time, the cells stay symmetric in each chamber. Then the cells in the upper chamber become asymmetric before merging into a single cell. There is a time delay before the lower chamber behaves exactly like the upper one, exhibiting a single cell. At large τ, the fluid in the chambers has accelerated enough to drive the fluid in vent by entrainment/shear.

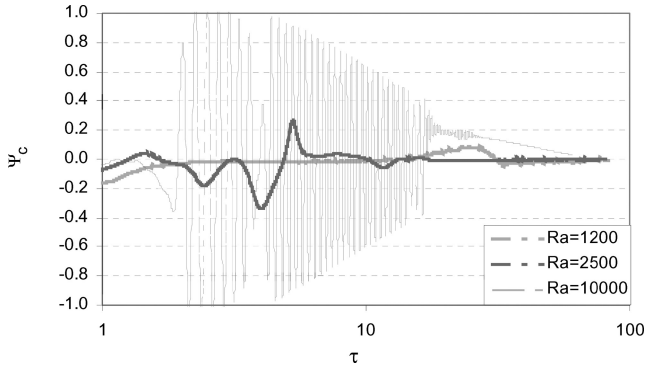

Fig. 4 Time trace of instantaneous vertical velocity (Ψ_c) for conduction, countercurrent, and oscillatory regimes.

This singular phenomenon of no flow at low Ra numbers is analogous to the Benard convection problem. At $\tau = 0$ fluid is at rest everywhere and the vent marks the region of separation of large bodies of hot and cold fluid. With respect to the vent, the denser fluid is at the top, with a natural tendency to exchange its place with the lighter fluid at the bottom of the vent. However, this exchange is inhibited by its own viscosity and for the flow to ensue, the adverse temperature gradient must exceed a certain value. The onset of instability beyond a critical value of the Rayleigh number has been thoroughly analyzed using techniques such as linear stability theory and the power integral method. Chandrasekhar[21] has presented a comprehensive treatment of the linear stability theory where he has shown mathematically the thermodynamic significance of Ra_{critical}. In his words: "Instability occurs at the minimum temperature gradient at which a balance can be steadily maintained between the kinetic energy dissipated by viscosity and the internal energy released by the buoyancy force." Ra_{critical} corresponds to this minimum temperature gradient in conjunction with the dynamical conditions at the two bounding planes. For the case of rigid constant temperature surfaces, Ra_{critical} has been calculated to be 1708; for one rigid and one free surface it is 1100; and for both free surfaces Ra_{critical} is found to be 658. The same line of reasoning can be applied to the flow in the vent. This is justified if one takes a closer look at Fig. 6, which shows a magnified view of velocity vectors in the vent. The following observation can be made. The magnitude of velocity in the vent is extremely small as compared to those in the enclosures. In the middle of the vent, velocities are negligible suggesting that the fluid movement at the top and bottom edges of the vent is due to bulk fluid motion in the enclosures. Two planes of symmetry exist dividing the vent into four similar parts. Several

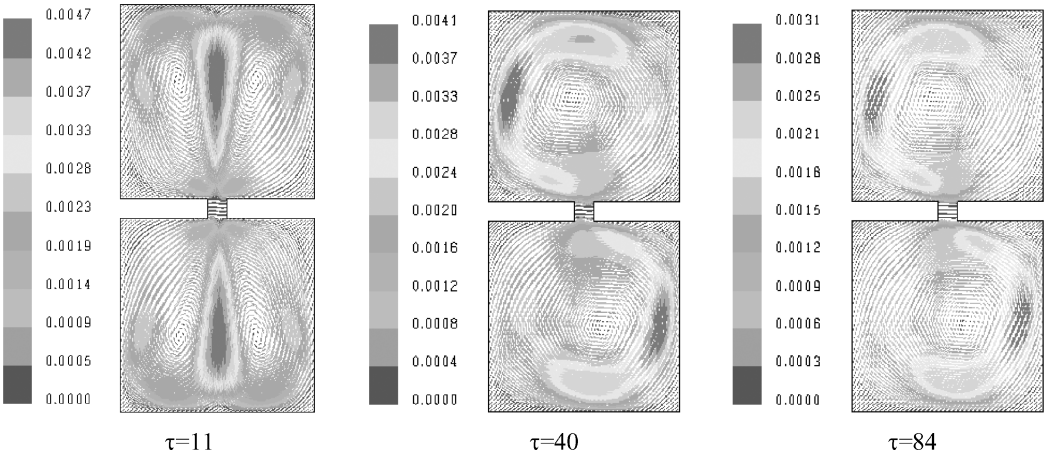

Fig. 5 Overall velocity field for $Ra = 1000$ (colored by velocity magnitude).

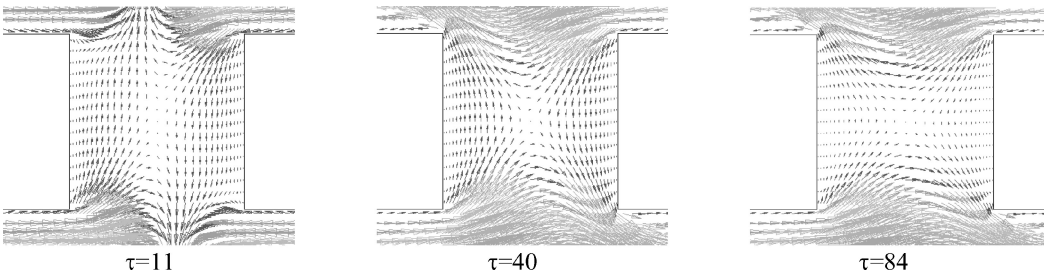

Fig. 6 Magnified view of the velocity field in the vent for $Ra = 1000$.

complications arise in this problem, which makes stability analysis difficult. One is the effect of sidewalls and the other is the influence of bulk fluid motion in upper and lower chambers, the latter being more complex than the former. To date, several researchers have addressed the issue of the effect of sidewalls on Ra_{critical}. The first complete analysis was given by Yih[22] for the stability of a viscous fluid between insulated vertical plates. Davis[19] was the first to consider a fully confined fluid. He used the Galerkin method for his analysis. Later Catton[23] improved on his results and produced a chart for Ra_{critical} as a function of $H1$ and $H2$ as parameters, where $H1$ and $H2$ are spanwise dimension and depth respectively. Both studies considered the sidewalls to be perfectly conducting walls. Later, Catton and Edwards[24] performed an experimental study on the effects of sidewalls on natural convection. They were able to obtain Ra_{critical} as a function of height to width ratio for insulating as well as conducting lateral walls. For an aspect ratio of 1.0 and insulating lateral walls, they reported that Ra_{critical} was in the range of 1×10^4 and 2×10^4. They also developed a heat transfer correlation.

On the second issue mentioned, regarding the influence of bulk fluid motion in enclosures on the vent, no prior works exist. Figures 7 and 8 give the change in θ_{av} on right and left walls of the vent respectively as a function of time. Instantaneous bulk (mass-weighted average) nondimensionalized temperature (θ_b) along a cross section on the center of the vent at $L/2$ is given by Fig. 9 and the instantaneous mass-weighted average velocity magnitude (Ψ_b) is shown by Fig. 10. In all figures mentioned above results for Ra of 1200 and 1300 are shown to demonstrate the process the authors went through to find the limiting Ra for different regimes.

For very small values of τ, a sharp gradient appears in (Ψ_b) because of the initial conditions imposed in the enclosures. However, the flow adjusts itself quickly to decrease this gradient as (θ_b) steadily decreases with time. Because all the heat transfer is by conduction only, the average wall temperature θ_{av} has a constant value of about 0.5 for all values of τ.

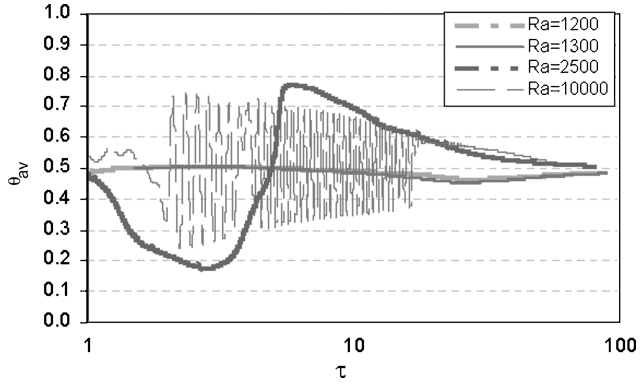

Fig. 7 Time trace of θ_{av} on the right wall of the vent.

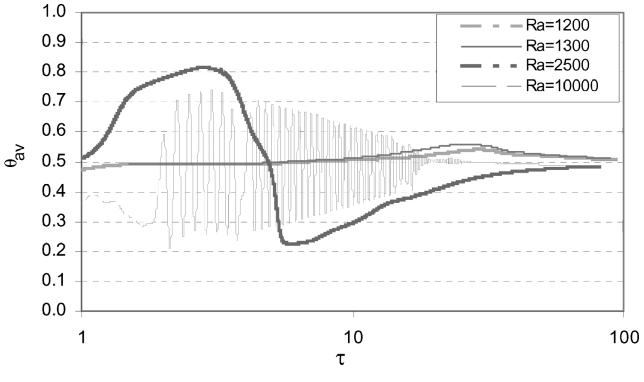

Fig. 8 Time trace of θ_{av} on the left wall of the vent.

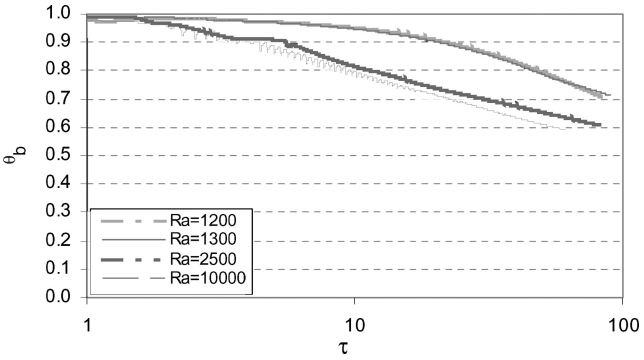

Fig. 9 Time trace of instantaneous bulk (mass-weighted average) nondimensionalized temperature (θ_b).

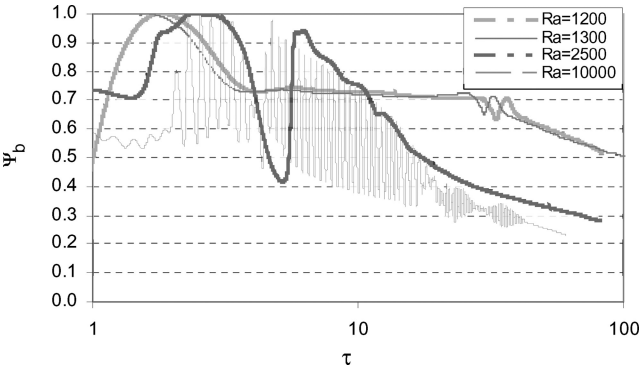

Fig. 10 Time trace of instantaneous mass-weighted average velocity magnitude (Ψ_b).

The Countercurrent Regime ($1600 \leq Ra < 3600$)

This regime is characterized by a downflow along approximately one-half of the vent and upflow along the rest to satisfy continuity, as can be seen in Fig. 11.

One essential difference in the flow patterns between $Ra = 1000$ and 2500 (Figs. 5 and 11) is that the cells in the top chamber for $Ra = 2500$ become asymmetric at early nondimensional times. This asymmetry arises at $\tau = 5.0$ during the onset of the countercurrent flow at the vent. A closer look at the vent (Fig. 12) clearly shows the upflow on the right side and downflow on the left side of the vent at $\tau = 2.2$. With time, the flow gradually reverts itself to the conduction regime with one large cell in each chamber as seen for $Ra = 1000$.

As Rayleigh number is increased in this flow regime, the flow patterns present the most interesting phenomenon. In Fig. 11 at $\tau = 2.2$, the flow patterns are strictly countercurrent in the vent; however, at $\tau = 8$, the flow everywhere in the enclosure slows down. This is evident from the magnified view of the vent in Fig. 12. Following this deceleration, a flow reversal occurs at the vent at $\tau = 11$ and lasts as seen at $\tau = 19$ and the flow accelerates again, as evident from the magnitude of velocity vectors. This is the only flow reversal that occurs in this flow regime.

Such a phenomenon was also seen by Myrum.[16] He conducted an experimental study to find the effect of vent size and Ra on natural convection heat transfer from a heated disk. This disk was located at the bottom of a top-vented enclosure. During the experiments, he also studied the flow patterns in the vent and reported four basic modes. In mode I, flow exited the vent along its axis and entered around its circular perimeter. In mode II, regions of outflow and inflow formed concentric rings within the vent. In mode III, inflow occurred through one half of the vent along the perimeter and corresponding outflow through the rest. A nonperiodic shift in sides of inflow and outflow was also observed as seen in the current flow situation.

Although a direct comparison cannot be made of the current study and Myrum's,[16] the time history of heat transfer along with numerical flow visualization reveal mode III. At the time of this change

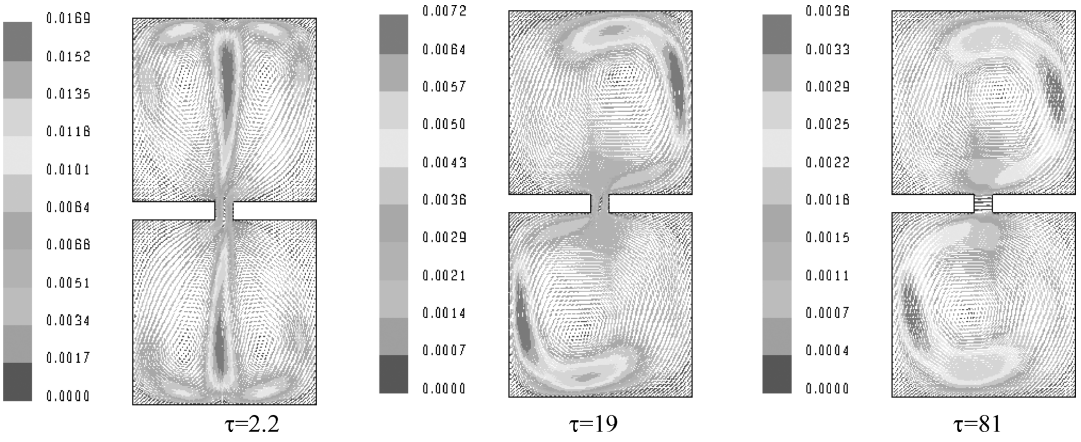

Fig. 11 Overall velocity field for *Ra* = 2500 (colored by velocity magnitude).

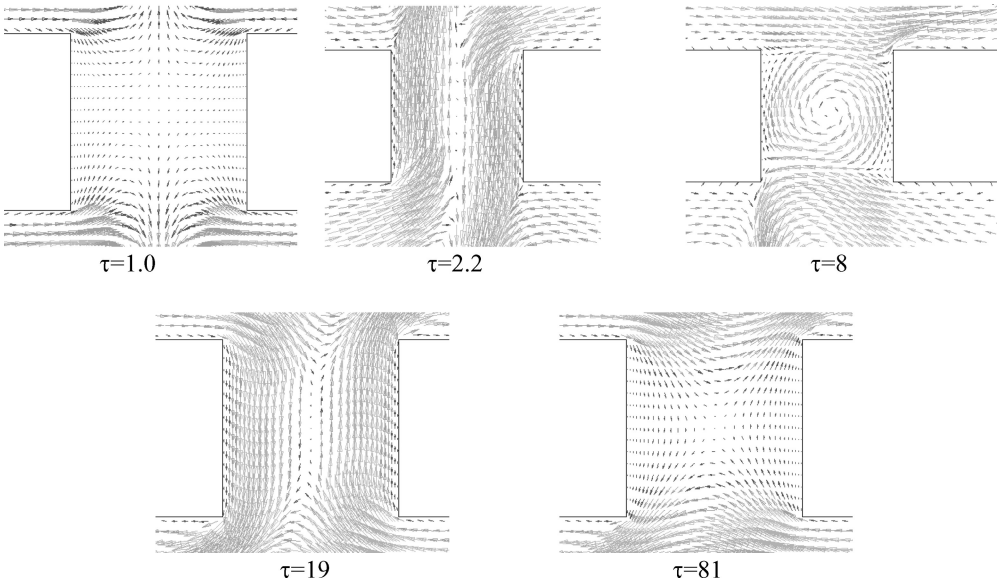

Fig. 12 Magnified view of the velocity field in the vent for *Ra* = 2500.

in direction near $\tau = 8$ as discussed above, the exchange flow rate decreases drastically with corresponding decrease in heat transfer across the vent as seen in Figs. 9 and 10. This change, therefore, appears in θ_b and Ψ_b time history as a sudden decrease. A sharp decrease and increase in the rate of change of instantaneous θ_{av} on the right and left walls of the vent respectively occur as shown by Figs. 7 and 8, due to the flow reversal. As soon as the change in sides is complete, the average and bulk temperatures and velocities resume at almost the same values as before the change. At large values of τ, flow in the vent gradually dies out due to lack of driving potential, namely the bulk mean temperature difference between the two enclosures. As this happens, the plumes are no longer strong enough to sustain two cells on either side and gradually the two cells merge to form a single cell. Because at this point of time there is no flow across the vent, the heat transfer is by conduction only. Hence the flow configuration is exactly as seen in Fig. 5 for large τ. Figures 4, 7, and 8 confirm this observation, where Ψ_c and θ_{av} are the same as for the conduction regime.

The Oscillatory Flow Regime (*Ra* ≥ 3600)

This regime is characterized by sudden bursts of both upflow and downflow. This shows up as a periodiclike response in Ψ_c, Ψ_b, and θ_{av}, θ_b time history for large Ra numbers only. This type of flow originates at nearly $Ra = 3600$.

The oscillatory flow with a single cell in the vent is dominant at high Rayleigh numbers of 5000, 10,000, and 50,000. The flow patterns are qualitatively similar and hence the flow and temperature time traces for $Ra = 10{,}000$ and the flow patterns for $Ra = 50{,}000$ in the enclosures and the magnified vent have been chosen for discussion and are given in Figs. 13 and 14. Unlike the other two regimes, the flow in the bottom chamber reaches a unicellular pattern earlier than the top enclosure. A close look at the flow patterns within the vent for $Ra = 50{,}000$, as given in Fig. 14, reveals that the cell that develops in the vent persists for a longer period before they undergo a flow reversal as seen before. Temperature and velocity plots for $Ra = 10{,}000$ at different times (Figs. 4, 7–10) give a unique perspective on occurrences in the vent. Temperature and velocity inversions occur at different times corroborating the fact that the flow oscillates with a well-defined frequency in the entire domain.

It is suspected that these bursts are periodic in nature and the frequency of bursts is a function of driving potential. Time traces of Ψ_c, Ψ_b and θ_{av}, θ_b for $Ra = 10{,}000$ (Figs. 4, 7–10) suggest that there are varying-amplitude oscillations in a narrow frequency range that eventually die out and essentially reproduce the flow behavior quantified in the countercurrent and conduction-flow regimes at large nondimensional time. The Nusselt number trace was observed by Mitchell and Quinn[25] in a confined layer heated from below. They found that as the plate temperature was increased, the fluid oscillated in a narrow frequency band. They also noted that the oscillations were stable over a large Rayleigh number range. Once again, a direct comparison of our results with those of Mitchell and Quinn[25] cannot be made because their mean flow was steady.

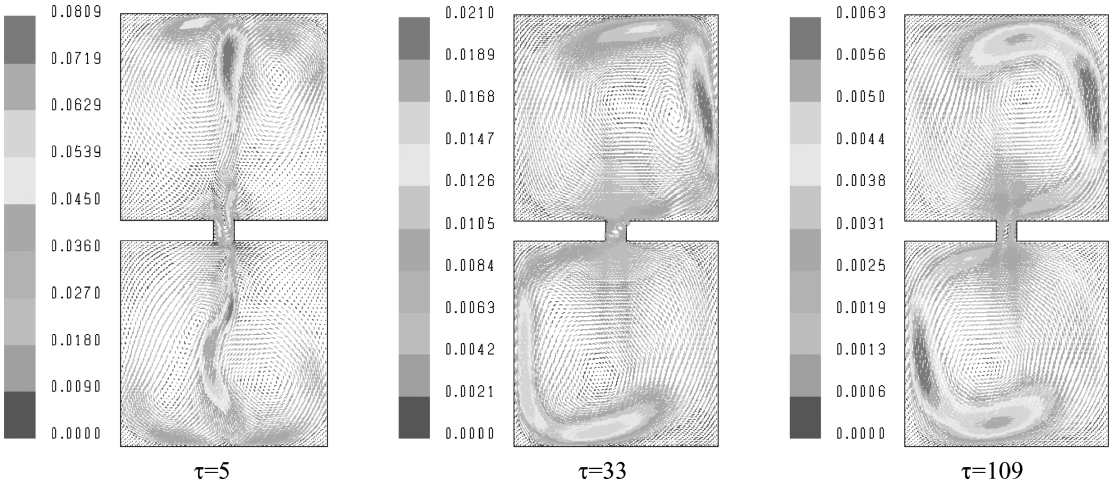

Fig. 13 Overall velocity field for *Ra* = 50,000 (colored by velocity magnitude).

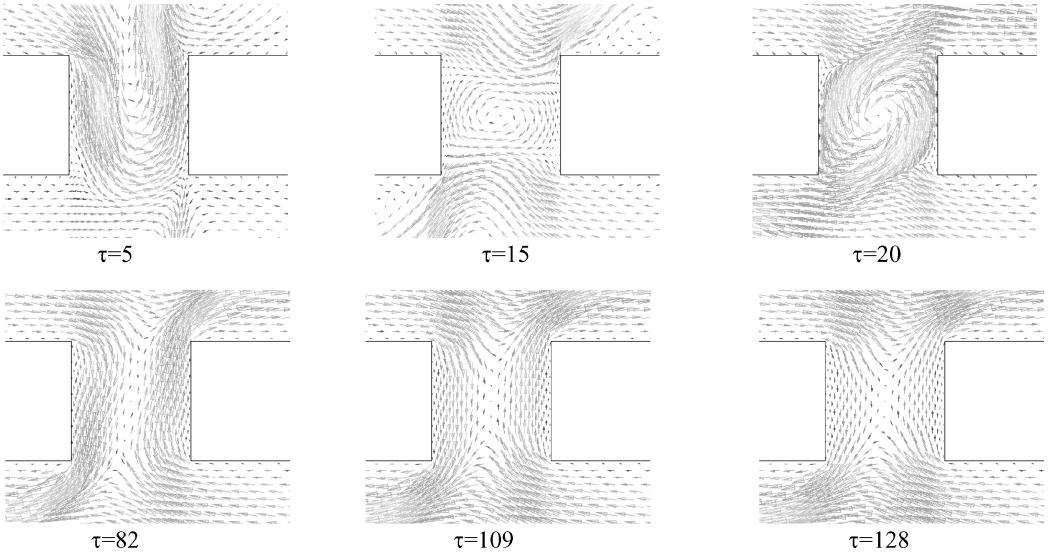

Fig. 14 Magnified view of the velocity field in the vent for *Ra* = 50,000.

Conclusions

A numerical study of unsteady, laminar, buoyant flow through a horizontal rectangular vent between two large enclosures was performed. Based on the flow patterns in the vent and the corresponding modes of heat transfer through it, three flow regimes were identified: the conduction regime ($Ra \leq 1500$), the countercurrent flow regime ($1600 \leq Ra < 3600$), and the oscillatory flow regime ($Ra \geq 3600$). In the conduction regime there is no flow across the vent, the viscous forces being as large as the buoyancy forces. This is analogous to the Benard convection problem, where the Rayleigh number must exceed a critical value before the flow can start, as explained analytically by Chandrasekhar[21] using linear stability theory. However, no closed form solution is available for the configuration under investigation to determine the exact value of critical Ra. In the countercurrent flow regime, the fluid moves through the vent in two distinct streams with one going up and the other going down. A flow reversal takes place in the vent soon after flow initiation, associated with a flow deceleration and a significant decrease and increase in the rate of change of instantaneous θ_{av} on the right and left walls of the vent, respectively. As soon as the change in sides is complete the average and bulk temperatures and velocities resume at almost the same values as before the change. Such a phenomenon was also observed in a similar flow situation by Myrum,[15] although in his case, the reversal occurred in a random manner. The third regime is characterized by sudden bursts of upflow and corresponding downflow with a well-defined frequency range. Temperature and velocity results associated with such bursts display interesting characteristics of increasing amplitudes but nearly the same frequency. Such oscillations were also documented by Mitchell and Quinn[25] for a steady mean-flow convection experiment in an unvented enclosure.

References

[1]Jaluria, Y., *Natural Convection Heat and Mass Transfer*, Pergamon, Oxford, 1980.

[2]Prahl, J., and Emmons, H. W., "Fire Induced Flow through an Opening," *Combustion and Flame*, Vol. 25, July 1975, pp. 369–385.

[3]Leach, S., and Thompson, H., "An Investigation of Some Aspects of Flow into Gas Cooled Nuclear Reactors Following an Accidental Depressurization," *Journal of British Nuclear Energy Society*, Vol. 14, 1975, pp. 243–250.

[4]Brown, W., "Natural Convection Through Rectangular Openings in Partitions. 2. Vertical Partitions," *International Journal of Heat and Mass Transfer*, Vol. 5, June 1962, pp. 295–299.

[5]Brown, W., and Salvason, K., "Natural Convection through Rectangular Openings in Partitions. 1. Vertical Partitions," *International Journal of Heat and Mass Transfer*, Vol. 5, June 1962, pp. 859–868.

[6]Epstein, M., "Buoyancy Driven Exchange Flow through Small Openings in a Horizontal Partition," *Journal of Heat Transfer*, Vol. 110, Jan. 1988, pp. 885–893.

[7]Mercer, A., and Thompson, H., "An Experimental Investigation of Some Further Aspects of the Buoyancy-Driven Exchange Flow between Carbon Dioxide and Air Following a Depressurization Acceident in a Magnox

Reactor. 1. The Exchange Flow in Inclined Ducts," *Journal of British Nuclear Energy Society*, Vol. 14, Oct. 1975, pp. 327–334.

[8]Gardner, G., "Motion of Miscible and Immiscible Fluids in Closed Horizontal and Vertical Ducts," *International Journal of Multiphase Flow*, Vol. 3, July 1977, pp. 305–318.

[9]Conover, T. A., and Kumar, R., "LDV Study of Buoyant Exchange Flow through a Vertical Tube," *Proceedings of 5th International Conference on Laser Anemometry, Advances and Applications*, The International Society for Optical Engineering (SPIE), Bellingham, WA, 1993.

[10]Conover, T. A., Kumar, R., and Kapat, J. S., "Buoyant Pulsating Exchange Flow through a Vent," *Journal of Heat Transfer*, Vol. 117, July 1995, pp. 641–648.

[11]Steckler, K., Baum, H., and Quintiere, J., "Fire Induced Flows through Room Openings—Flow Coefficients," *Twentieth Symposium (International) on Combustion*, The Combustion Institute, Pittsburgh, PA, 1984.

[12]Steckler, K., Baum, H., and Quintiere, J., *Twenty-First Symposium (International) on Combustion*, The Combustion Institute, Pittsburgh, PA, 1986.

[13]Tan, Q., and Jaluria, Y., "Flow through a Horizontal Vent in an Enclosure Fire," *Fire and Combustion Systems, ASME HTD*, Vol. 199, Aug. 1992, pp. 115–122.

[14]Jaluria, Y., Lee, S. H.-K., Mercier, G. P., and Tan, Q., "Visualization of Transport across a Horizontal Vent Due to Density and Pressure Difference," *Visualization of Heat Transfer Processes*, ASME HTD, New York, 1993.

[15]Myrum, T., "Natural Convection from a Heat Source in a Top-Vented Enclosure," *Journal of Heat Transfer*, Vol. 112, Jan. 1990, pp. 632–639.

[16]Singhal, M., and Kumar, R., "Unsteady Buoyant Exchange Flow through a Horizontal Partition," *Journal of Heat Transfer*, Vol. 117, Jan. 1995, pp. 515–520.

[17]Patankar, S. V., *Numerical Heat Transfer and Fluid Flow*, Hemisphere Publishing Co., New York, 1980.

[18]Patterson, J., and Imberger, J., "Unsteady Natural Convection in a Rectangular Cavity," *Journal of Fluid Mechanics*, Vol. 100, Aug. 1980, pp. 65–86.

[19]Davis, G. De Vahl, "Natural Convection of Air in a Square Cavity: A Bench Mark Numerical Solution," *International Journal of Numerical Methods in Fluids*, Vol. 3, June 1983, pp. 249–264.

[20]Bejan, A., *Convection Heat Transfer*, Wiley, New York, 1984.

[21]Chandrasekhar, S., *Hydrodynamic and Hydromagnetic Stability*, Clarendon, London, 1961.

[22]Yih, C. S., "Thermal Instability of Viscous Fluids," *Quarterly of Applied Mathematics*, Vol. 17, July 1959, p. 25.

[23]Catton, I., "Convection in Closed Rectangular Region: The Onset of Motion," *Journal of Heat Transfer*, Jan. 1970, pp. 186–188.

[24]Catton, I., and Edwards, D. K., "Effect of Side Walls on Natural Convection Between Horizontal Plates Heated from Below," *Journal of Heat Transfer*, Jan. 1967, pp. 295–299.

[25]Mitchell, W. T., and Quinn, J. A., "Thermal Convection in a Completely Confined Fluid Layer," *AIChE Journal*, Vol. 12, Aug. 1966, pp. 1116–1124.